

MAGNETIC RECONNECTION RATE AND FLUX-ROPE ACCELERATION OF TWO-RIBBON FLARES

JU JING, JIONG QIU, JUN LIN, MING QU, YAN XU, AND HAIMIN WANG

Center for Solar Terrestrial Research, New Jersey Institute of Technology, Dr. Martin Luther King Boulevard, Newark, NJ 07102

Received 2004 September 8; accepted 2004 November 1

ABSTRACT

Forbes & Lin derived simple equations to link the properties of magnetic reconnection in the corona to observed signatures of solar flares. We measured the photospheric magnetic fields and the flare ribbon separation speeds then applied these equations to derive two physical terms for the magnetic reconnection rates: the rate of magnetic flux change φ_{rec} involved in magnetic reconnection in the low corona and the electric field E_{rec} inside the reconnecting current sheet (RCS) that is generated during magnetic reconnection. The central interest in this work is to investigate and quantify the statistical correlation between the magnetic reconnection rate and the corresponding flux-rope acceleration. From a sample of 13 well-observed two-ribbon flares, which are associated with filament eruptions or coronal mass ejections (CMEs), the acceleration of erupting filaments is found mainly in the range of $0.05\text{--}0.4\text{ km s}^{-2}$, up to 3 km s^{-2} . Correspondingly, the maximum E_{rec} and φ_{rec} mostly occur in the range of $0.2\text{--}5\text{ V cm}^{-1}$ and $0.5\text{--}6 \times 10^{18}\text{ Mx s}^{-1}$, respectively. A positive and strong correlation is found with a cross-correlation coefficient of $0.94\text{--}0.97$ between the magnetic reconnection rate and the acceleration of erupting filaments that represents the early stages of flux-rope eruptions in the low corona. However, the inferred reconnection rate is not correlated to the acceleration of CME fronts measured by the Large Angle and Spectrometric Coronagraph (LASCO) observations in the range of $2\text{--}30$ solar radii (the correlation coefficient is less than 0.2). A reasonable correlation is found between the reconnection rate and the velocity of CMEs, which indicates the cumulative acceleration of CMEs from the low corona to the LASCO C2 field of view. The temporal correlation between the magnetic reconnection rate and the flare nonthermal emissions has also been verified in this paper.

Subject headings: Sun: coronal mass ejections (CMEs) — Sun: filaments — Sun: flares — Sun: magnetic fields

1. INTRODUCTION

Numerous theoretical models for solar eruptions and the evolution of the reconnecting current sheet (RCS) have been developed (e.g., Van Tend & Kuperus 1978; Kaastra 1985; Martens & Kuin 1989; Forbes & Priest 1995; Amari et al. 1996; Forbes & Lin 2000; Choe & Cheng 2000; and see Lin 2003 for a review). These models can be arranged into four categories: (1) non-force-free models, (2) ideal MHD models, (3) resistive MHD models, and (4) ideal-resistive hybrid models. Some of the most used eruption models are the sheared arcade model (Mikić et al. 1988; Linker & Mikić 1994), the breakout model (Antiochos et al. 1999), and the flux-rope catastrophic model (Van Tend & Kuperus 1978; Forbes & Isenberg 1991; Forbes & Priest 1995). The first two eruption models are of the resistive MHD model type and, on the basis of numerical simulation, require magnetic reconnection to trigger the eruption. The third eruption model, constructed via analytic solution of the ideal-resistive hybrid model, indicates quantitatively that magnetic reconnection does not necessarily play an essential role in triggering a catastrophic eruption. However, magnetic reconnection does help a catastrophe develop into a plausible CME-like eruption, as well as giving rise to intense heating that accounts for the associated flares (Lin 2001; Lin et al. 2001).

Observationally, solar eruptions can be manifested in the form of ejected X-ray plasmas, erupting filaments, or coronal mass ejections (CMEs) (Cheng et al. 2003). The morphological evolution of two-ribbon flares, characterized by two bright separating ribbons in the chromosphere, usually occurs during the solar eruptive phenomena (eruptive filaments or CMEs) and is believed to be the lower atmosphere manifestation of magnetic reconnection at progressively higher levels and the subsequent energy release in the corona (Choudhary & Gary 1999).

There is increasing observational evidence of a temporal correlation between flares and eruptive phenomena (Gosling et al. 1976; MacQueen & Fisher 1983; Zhang et al. 2001; Qiu et al. 2002, 2004; Wang et al. 2003). This correlation leads us to believe that flares, eruptive filaments, and CMEs are different manifestations of the same physical process involving magnetic reconnection.

Because eruptive filaments and CMEs are both considered to be erupting flux ropes in many theoretical models, we will not distinguish them except for a specific purpose. Instead, the term “flux-rope” is used throughout the rest of the paper. However, we must keep in mind that the occulting disk of coronagraphs block part of the lower corona. Consequently, the initial stage of a flux-rope eruption usually cannot be observed by coronagraphs such as the Large Angle Solar Coronagraph (LASCO; Brueckner et al. 1995).

In a simplified two-dimensional model, the release of energy during a flare occurs in a RCS formed at an X-type neutral line (Forbes & Priest 1984; Priest & Forbes 1986). The rate at which the magnetic flux is converted into the diffusion region, in terms of the electric field E_{rec} in the RCS, can be inferred by measuring the flare ribbon expansion speed V_r and the normal component of the magnetic field B_n swept by the flare ribbons: $E_{\text{rec}} = V_r B_n$ (Forbes & Priest 1984; Priest & Forbes 1986). More generally, Forbes & Lin (2000) considered the rate of photospheric magnetic flux change φ_{rec} instead of the electric field in the region of newly closed field lines. The flux change rate can be evaluated by the following equation (Forbes & Lin 2000):

$$\varphi_{\text{rec}} = \int E_{\text{rec}} dl = \frac{\partial}{\partial t} \int B_n da, \quad (1)$$

where dl is the length along the RCS and da is the newly brightened area swept by the flare ribbons.

E_{rec} and φ_{rec} provide a measure of the reconnection rate inside the current sheet, and the measurement itself is not dependent on specific models. In this manner, we are particularly interested in the observational signatures of two-ribbon flares that are associated with flux-rope eruptions. We can infer the reconnection rate and compare it with the rising motion of flux ropes. Essentially, the reconnection rate and the flux-rope acceleration focus on important features of the flare. “Flux-rope” models, therefore, provide a stringent test of the scenarios in which the ejection of solar material and magnetic reconnection are physically linked. Progress in this research area has been made recently by Lin & Forbes (2000) and Qiu et al. (2004).

The central interest in this work is to find statistical correlation between the magnetic reconnection rate and the acceleration of flux ropes. From a sample of 13 well-observed two-ribbon flares that are associated with rising flux ropes, there appears to be a tendency that increasing reconnection rates are usually associated with increasing flux-rope accelerations at the early stage. The temporal correlation between the magnetic reconnection rate and the flux-rope acceleration has also been verified in this paper.

The data sets and methods of analysis are described in §§ 2 and 3, respectively. In § 4, on the basis of a sample of 13 two-ribbon flares that are associated with eruptive flux ropes, we quantify the correlation between magnetic reconnection rates and flux-rope accelerations. Finally, our observational results are summarized and briefly discussed in § 5.

2. THE DATA SETS

We used Big Bear Solar Observatory (BBSO) $H\alpha$ full-disk images as the primary data source to trace the flare ribbon expansion and the filament rising motion. BBSO $H\alpha$ observations are suitable because of their high cadence (one or more image frames per minute), high resolution (approximately $1''$ pixel $^{-1}$), and superior detail and contrast (Martin 1989). In the cases in which there were data gaps in the BBSO observations, we resorted to $H\alpha$ full-disk images obtained at Kanzelhöhe Solar Observatory (KSO) in Austria, which is a station in our global $H\alpha$ network. In addition, an X10.0 white-light flare that occurred on 2003 October 29, obtained at the National Solar Observatory, Sacramento Peak, was also added to our study list. Running difference images from the Extra-Ultraviolet Imaging Telescope (EIT), on board the *Solar and Heliospheric Observatory* (SOHO), were used to supplement $H\alpha$ data in identifying the height of the rising filament in the cases in which the filaments’ motion could not be determined unambiguously from $H\alpha$ observations.

The CME height-time data are provided by the LASCO Web site that has been compiled by S. Yashiro and G. Michalek under the guidance of N. Gopalswamy.¹ Michelson Doppler Imager (MDI) magnetograms were used to measure the longitudinal component of the magnetic fields, which approximate the normal component of the magnetic field B_n because all the flares in our study occur near the disk center. Additionally, light curves from the *Geostationary Operational Environmental Satellite* (GOES) soft X-ray, *Yohkoh* and *RHESSI* hard X-ray, and Owens Valley Solar Array (OVSA) microwave data were also collected to study the evolution of flare emissions. If no hard X-ray and microwave observations were found, which was the case for some of the events that are under discussion, we used the time derivative of the GOES soft X-ray light curve to

indicate the evolution of flare nonthermal emission (Neupert 1968).

3. DATA ANALYSIS

As we discussed in the introduction, the magnetic reconnection rate can be deduced by measuring the expansion of flare ribbons across the magnetic field. We recently developed an image segmentation technique, which applies “region growing” and “adaptive boundary-base” methods (Jahne 1997; Gonzalez & Woods 2002) to derive the expansion speed of two-ribbon flares V_r and the newly brightened areas swept by flare ribbons da automatically (for more details, see Qu et al. 2003, 2004). From V_r and da , one may derive two forms of the magnetic reconnection rate: the electric field inside the RCS, $E_{\text{rec}} = V_r B_n$, and the rate of magnetic flux participating in the reconnection, $\varphi_{\text{rec}} = (\partial/\partial t) \int B_n da$. Uncertainties in E_{rec} and φ_{rec} caused by the influence of background noise were estimated to be less than 40% at the time of the peak value (Qu et al. 2004). Methods and uncertainties of these measurements are discussed in detailed by J. Qiu et al. (in preparation).

The velocity and acceleration of the filaments and CMEs are derived numerically as the first and second derivatives of corresponding height with respect to time. The uncertainty of measuring the filament height is estimated to be less than 4 pixels in each image, depending on the sharpness of the rising front. The typical rise phase of a filament lasts tens of minutes, and our $H\alpha$ observations have a regular cadence from 20 s to 1 minute. With the sufficient number of $H\alpha$ images and observational evidence (Wang 2005), we can straightforwardly assume that filament trajectories follow a linear growth during this period. In this case, the uncertainty in the values of filament velocity and filament acceleration arise both from the uncertainty and the time interval in measuring the filament height; the larger the uncertainty in the height and the shorter the time interval, the larger the uncertainty of the estimated values. The uncertainty in CME heights and speeds are estimated to be less than 5% and 10%, respectively. However, the cadence of LASCO observations (around 30 minutes) limits our estimation of the propagation of the uncertainty to some extent. In other words, a few of the measurements of CME heights, as well as a lack of evidence that CMEs display a constant acceleration at the initial stage of eruption, yields a very large uncertainty in the CME acceleration.

4. RESULTS

The events under study were selected on the basis of the following criteria: (1) disk events, (2) continuous and complete observation of the flares and the associated flux-rope rising motions, and (3) exhibiting clear flare expansion and, if present, filament rising motion. Criterion 1 follows from the fact that, for disk events, B_n can be easily measured as the longitudinal component provided in MDI magnetograms. Criteria 2 and 3 are required because we need track the outer edge of flare ribbons and the rising fronts of eruptive filaments to infer the magnetic reconnection rate and acceleration of the filaments.

We found 13 two-ribbon flare events that satisfy all three criteria. They are listed in Table 1. All but one event are well observed by BBSO or KSO $H\alpha$ images. The exception is the X10.0 flare in NOAA Active Region 10486, which was observed in the near-infrared (NIR) continuum at $1.56 \mu\text{m}$ (Xu et al. 2004). These events are classified into three groups (col. [2]) by their associated eruptive phenomena: group A consists of two-ribbon flares with both eruptive filaments and

¹ Available at http://cdaw.gsfc.nasa.gov/CME_list/.

TABLE 1
LIST OF EVENTS IN THIS STUDY

EVENT (1)	GROUP ^a (2)	DATE (3)	FLARE						FILAMENT	CME	
			Class (4)	NOAA ^b (5)	Begin (6)	Peak (7)	End (8)	Location (9)	Rising Time (10)	Time ^c (UT) (11)	Comment (12)
1.....	A	2000 Sep 12	M1.0	QS ^d	11:31	12:13	13:13	S12 W18	10:30–12:00	11:54	Halo
2.....	A	2000 Sep 27	optical ^c	QS ^d	S31 E17	19:30–19:50	20:50	Loop with looplike core
3.....	A	2001 Apr 23	C2.8	9431	12:06	12:23	12:36	S14 W17	12:02–12:18	12:40	Loop front with cavity and core
4.....	A	2001 Oct 19	X1.6	9661	16:13	16:30	16:43	N15 W29	16:15–16:25	16:50	Halo
5.....	A	2002 May 21	M1.5	9960	21:20	21:39	22:00	N17 E38	20:16–20:26	21:50	Loop front with cavity and trailing material
6.....	A	2003 May 27	X1.3	0365	22:56	23:07	23:13	S07 W17	22:58–23:04	23:26	Halo
7.....	A	2004 Mar 4	optical ^c	QS ^d	N20 W10	19:50–21:00	22:30	Loop front
8.....	A	2004 Mar 30	C2.0	0581	22:53	23:08	23:45	S05 E02	22:30–22:46	no data ^f	...
9.....	B	2000 Feb 17	M2.5	8869	18:41	18:52	19:05	S25 W16	18:56–19:28
10.....	B	2002 Aug 26	optical ^c	0087	S07 E20	21:00–21:40
11.....	C	2001 Aug 25	X5.3	9591	16:23	16:45	17:04	S17 E34	...	16:50	Halo
12.....	C	2002 Jul 26	M8.7	0044	20:51	21:12	21:29	S19 E26	...	22:06	Halo, cavity and core follow
13.....	C	2003 Oct 29	X10.0	0486	20:37	20:49	21:01	S15 W02	...	20:54	Halo

^a A: two-ribbon flare with rising filament and eruption and CME; B: two-ribbon flare with rising filament but no eruption and without CME; C: two-ribbon flare with CME but without apparent filament motion.

^b Active Region number.

^c First C2 appearance time.

^d Quiescent area.

^e Flare visible in H α observations but is either inconspicuous in soft X-ray flux profiles or is of an insufficient magnitude to be officially classified as a flare.

^f No LASCO data.

CMEs; group B consists of two-ribbon flares with rising, not eruptive, filaments and without CMEs; and group C is composed of two-ribbon flares with CMEs but without apparent filament motion. Column (3) lists the date of the events. The subsequent columns provide instances of flares (cols. [4]–[9]), filaments (col. [10]), and CMEs (cols. [11]–[12]).

Table 2 summarizes the results deduced from the observations, including the maximum ribbon expansion speed (V_r , col. [3]), the maximum photospheric magnetic field strength (B_n , col. [4]), the maximum electric field in RCS (E_{rec} , col. [5]), the maximum magnetic flux change rate (φ_{rec} , col. [6]), the maximum filament acceleration (A_{fila} , column [7]), and the

TABLE 2
DATA TAKEN AND DEDUCED FOR EVENTS LISTED IN TABLE 1

EVENT (1)	DATE (2)	MAXIMUM VALUES								
		V_r (km s ⁻¹) (3)	B_n (Gauss) (4)	E_{rec} (V cm ⁻¹) (5)	φ_{rec} (10 ¹⁸ Mx s ⁻¹) (6)	A_{fila} (km s ⁻²) (7)	A_{CME} (km s ⁻²) (8)	ΔT_1^a (minutes) (9)	ΔT_2^b (minutes) (10)	ΔT_3^c (minutes) (11)
1.....	2000 Sep 12 ^d	25	200	0.5	2.0	0.2	0.4	-5	5	10
2.....	2000 Sep 27	11.4	46.4	0.24	0.5	0.14	0.2
3.....	2001 Apr 23	6.4	396.5	0.74	0.8	0.33	0.02	10	3	95
4.....	2001 Oct 19 ^d	74.7	308.0	21.0	14.7	3.0	0	-1	-5	...
5.....	2002 May 21	17.9	297.5	4.9	6.0	0.16	0.8	6	6	20
6.....	2003 May 27	65.3	387.5	14.4	8.7	1.8	0.02	-3	-5	40
7.....	2004 Mar 4	8.1	121.0	0.9	1.4	0.14	unavailable ^e
8.....	2004 Mar 30	30	200.0	2.5	0.7	0.12	no data ^f	8	-15	...
9.....	2000 Feb 17	13.0	195.1	1.4	2.3	0.3	...	25	24	...
10.....	2002 Aug 26	16	195.0	1.6	0.7	0.06
11.....	2001 Aug 25	25.8	461.5	8.9	4.9	...	0.4	-10	...	20
12.....	2002 Jul 26 ^g	19.0	334.5	2.8	6.0	...	-0.2	0	...	80
13.....	2003 Oct 29 ^h	63.8	919.6	37.8	10.8	...	0.06	-1	...	12

^a ΔT_1 = time of maximum E_{rec} - time of HXR at maximum. If no hard X-ray observation was found, the time derivative of the GOES soft X-ray light curve is used.

^b ΔT_2 = time of maximum A_{fila} - time of HXR at maximum.

^c ΔT_3 = time of maximum A_{CME} - time of HXR at maximum.

^d See Qiu et al. (2004) for a detailed case study.

^e CME height-time data of this event is not readily released at the SOHO LASCO Web site.

^f No LASCO data.

^g See Wang et al. (2004) for a detailed case study.

^h See Xu et al. (2004) for a detailed case study.

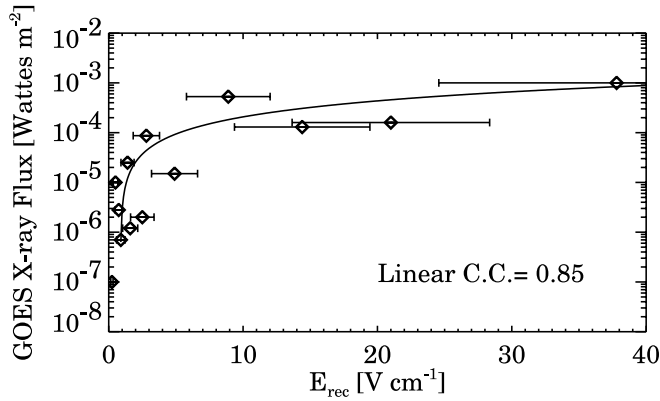


FIG. 1.—Scatter diagram of observed flare magnitude vs. derived maximum E_{rec} with estimated error bars. The solid line is a fit to the data points in the form of $\text{Flux} = -2.0 \times 10^{-5} + (2.3 \times 10^{-5})(E_{\text{rec}})$ with a correlation coefficient of 0.85.

maximum CME acceleration (A_{CME} , col. [8]). The last three columns of Table 2 list the time intervals of the E_{rec} , A_{fila} , and A_{CME} after the hard X-ray spike. If they peak after the time of the hard X-ray spike, the value is positive. Otherwise, the value is negative.

Our observational findings on the basis of sample events are described in detail as follows. Acceleration of erupting fila-

ments is mainly in the range of $0.05\text{--}0.4 \text{ km s}^{-2}$, up to 3 km s^{-2} . The maximum E_{rec} and φ_{rec} mostly occur in the range of $0.2\text{--}5 \text{ V cm}^{-1}$ and $0.5\text{--}6 \times 10^{18} \text{ Mx s}^{-1}$, respectively. In the case of the extremely dramatic flare on 2003 October 29, E_{rec} reaches a magnitude of about 38 V cm^{-1} . We found that the electric field is generally comparable with most observational results (Poletto & Kopp 1986; Wang et al. 2003, 2004; Qiu et al. 2004) and simulation results (Martens & Kuin 1989; Lin 2002; Cheng et al. 2003). The electric field strength found above implies strong heating and particle acceleration, which are responsible for the high-energy emissions (Cheng et al. 2003; Qiu et al. 2002, 2004). A graphical description of the derived maximum E_{rec} versus the observed magnitude of flares is shown in Figure 1. As expected, the magnitudes of the flares increase as E_{rec} increases with a high correlation coefficient (CC), 0.85.

In this study, erupting filaments are treated as proxies for the initial stages of rising flux ropes. The temporal correlation of the evolution of flare nonthermal emission, the magnetic reconnection rate, and the filament acceleration are examined and illustrated by one example in which an X1.3 flare occurred in NOAA Active Region 10365 on 2003 May 27 and was accompanied by a filament eruption and a halo CME. In $\text{H}\alpha$, the filament has a maximum acceleration of 1.8 km s^{-2} at 23:02 UT, and the bright flare ribbons appeared at 22:40 UT and lasted until 23:30 UT. In the LASCO observations, the CME was first apparent at 23:50 UT. Figure 2 displays the temporal

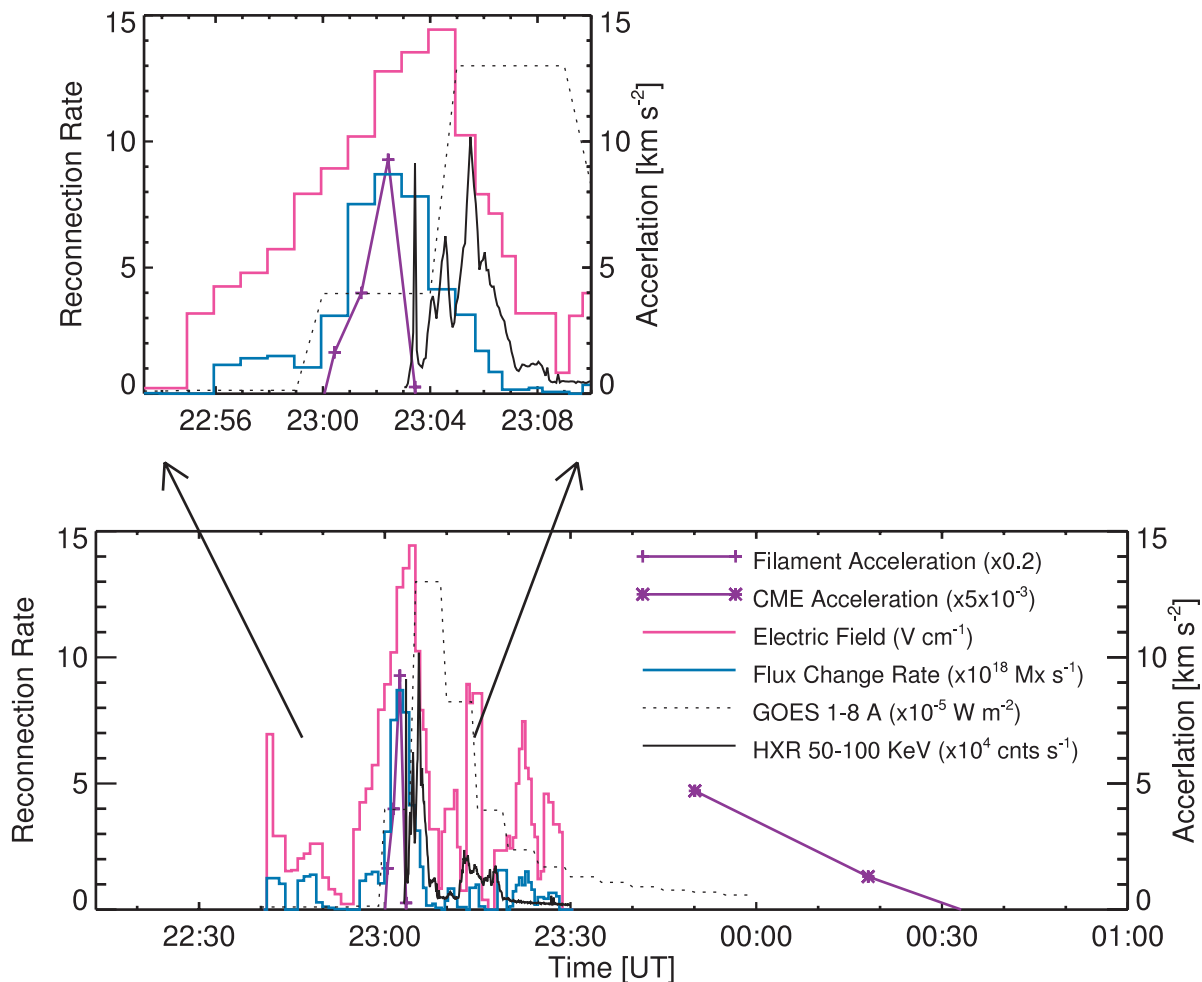


FIG. 2.—Temporal evolution of E_{rec} and φ_{rec} derived for the X1.3 flare on 2003 May 27, compared with the evolution of the acceleration of corresponding erupting filament and CME and soft X-ray and hard X-ray light curves. The top panel is the same as the bottom panel but is magnified for a selected time period.

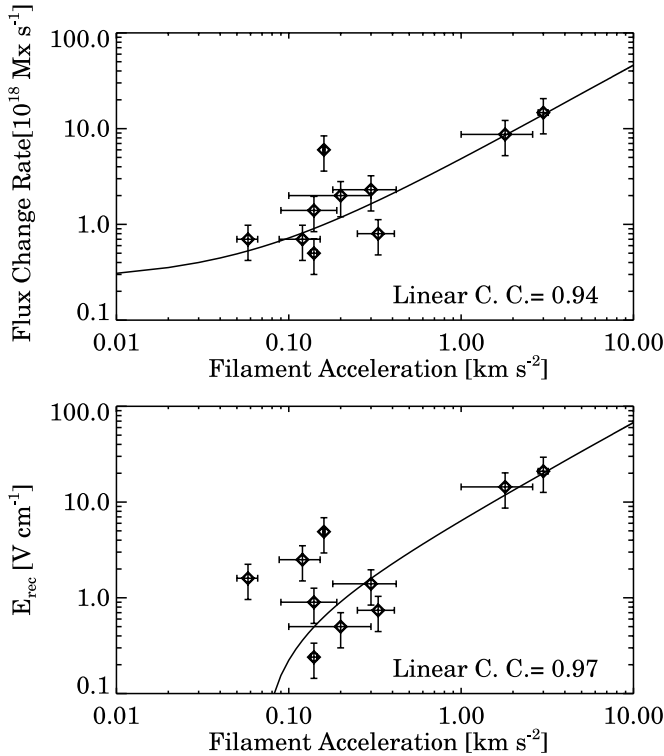


FIG. 3.—*Top*: Scatter diagram of maximum φ_{rec} vs. maximum filament acceleration in a logarithmic scale. The solid line is a fit to the data points of φ_{rec} and A_{fila} in the form of $\varphi_{\text{rec}} = 0.26 + 4.6A_{\text{fila}}$ with a correlation coefficient of 0.94. *Bottom*: Scatter diagram of maximum E_{rec} vs. maximum filament acceleration in a logarithmic scale. The solid line is a fit to the data points of E_{rec} and A_{fila} in the form of $E_{\text{rec}} = -0.46 + 6.8A_{\text{fila}}$ with a correlation coefficient of 0.97. Error bars attached to each point indicate the uncertainty of the measurement.

evolution of the inferred E_{rec} , φ_{rec} , accelerations of the corresponding erupting filament and CME, and the light curves of the *GOES* soft X-rays and *RHESSI* hard X-rays. The maximum E_{rec} , 14.4 V cm^{-1} , and the maximum φ_{rec} , $8.7 \times 10^{18} \text{ Mx s}^{-1}$, occur at 23:04 UT and 23:02 UT, respectively. The impulsive hard X-ray emission in the 50–100 keV energy band spikes at 23:03 and 23:07 UT. Apparently, E_{rec} , φ_{rec} , filament acceleration, and flare nonthermal emission reach their maximum values at almost the same time. It is necessary to point out that good temporal correlation generally exists for all events listed in Table 1, which confirms the findings of Qiu et al. (2004). These observations, which were in good quantitative agreement with some theoretical simulation results (Martens & Kuin 1989; Cheng et al. 2003), also indicate that the inferred macroscopic electric field in the RCS plays an important role in accelerating nonthermal particles to emit hard X-rays and microwaves (Qiu et al. 2004).

As we mentioned in § 1, the primary purpose of this work is to investigate the correlation between the magnetic reconnection rate and the flux-rope acceleration. To better illustrate our deduced results in Table 2, Figure 3 displays scatter diagrams of the reconnection rate (namely, E_{rec} and φ_{rec}) versus the acceleration of filaments in a logarithmic scale. Figure 4, for the purpose of comparison, plots the reconnection rate versus the acceleration of the CMEs. Those events without the corresponding filament motion or the CME are excluded from Figures 3 and 4. All values refer to the maxima that were found on each events. The error bars that are attached to each sign indicate the uncertainty of the measurement. Figure 3 shows that the increasing reconnection rate is usually associated with an increasing filament accelera-

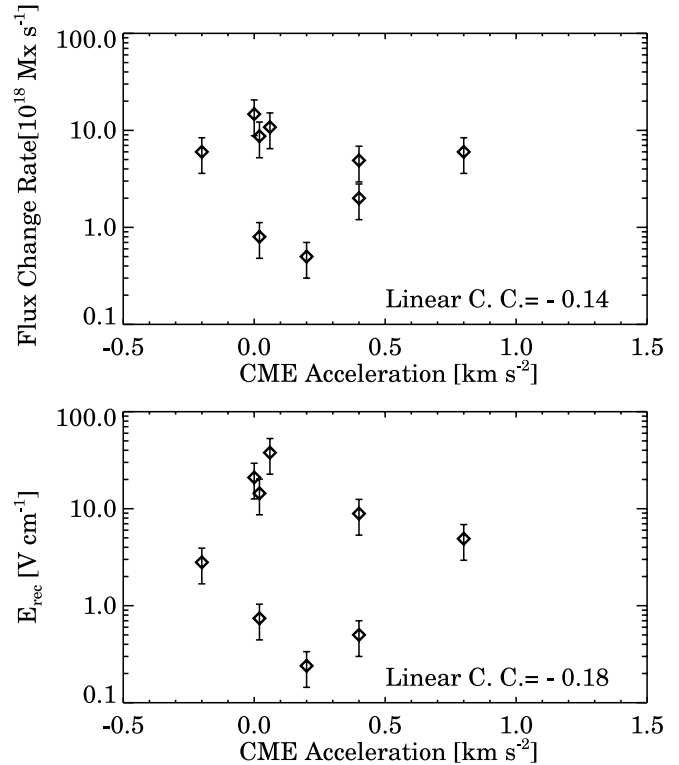


FIG. 4.—*Top*: Scatter diagram of maximum φ_{rec} with error bars vs. maximum CME acceleration in a logarithmic scale. *Bottom*: Scatter diagram of maximum E_{rec} with error bars vs. maximum CME acceleration in a logarithmic scale. The correlation coefficients are -0.14 and -0.18 , respectively. The error bars for the values of CME acceleration are not shown because they might be very large as a result of an insufficient number of measurements during the acceleration phase of the CMEs.

tion. More specifically, the linear CC between E_{rec} and A_{fila} is about 0.97, and that between φ_{rec} and A_{fila} is about 0.94. Such high values distinctly indicate a very strong correlation and a dependable relationship. The solid lines fit the paired data to linear models. The best-fit linear models are as follows: $E_{\text{rec}} = -0.46 + 6.8A_{\text{fila}}$, and $\varphi_{\text{rec}} = 0.26 + 4.6A_{\text{fila}}$. By contrast, Figure 4 shows a loose and irregular distribution of data points. Low CCs, -0.14 between φ_{rec} and A_{CME} and -0.18 between E_{rec} and A_{CME} , signify little, if any, correlation. This may stem from the fact that we were measuring the CME acceleration in the LASCO C2 and C3 fields of view ($2\text{--}30 R_{\odot}$) and hence did not sample the heights in the low corona. The insufficient number of measurements also implies a very large uncertainty in CME acceleration. As a result, the error bars for the values of CME acceleration are not shown in Figure 4.

It is suggested by Gopalswamy & Thompson (2000) that the acceleration of CMEs is strongly dependent on the altitudes at which the CMEs are observed. Specifically, Zhang et al. (2001) investigated the kinematic evolution of four CMEs in the lower corona and found that the acceleration of CMEs takes place from 1.3 to $4.6 R_{\odot}$. Similar results were also obtained by Shanmugaraju et al. (2003), who claimed that the peak in the acceleration mostly occurs below $3 R_{\odot}$. In this sense, the acceleration of most CMEs might decrease, or even stop, before they appear in LASCO C2 coronagraph images, by which time the velocity of the CMEs have obtained a nearly constant, or slightly decreasing, value. That is, the maximum acceleration of CMEs derived from LASCO C2 and C3 data is usually not really informative.

The velocity of CMEs at C2 might be useful because it is the cumulation of the CME acceleration at its early stage

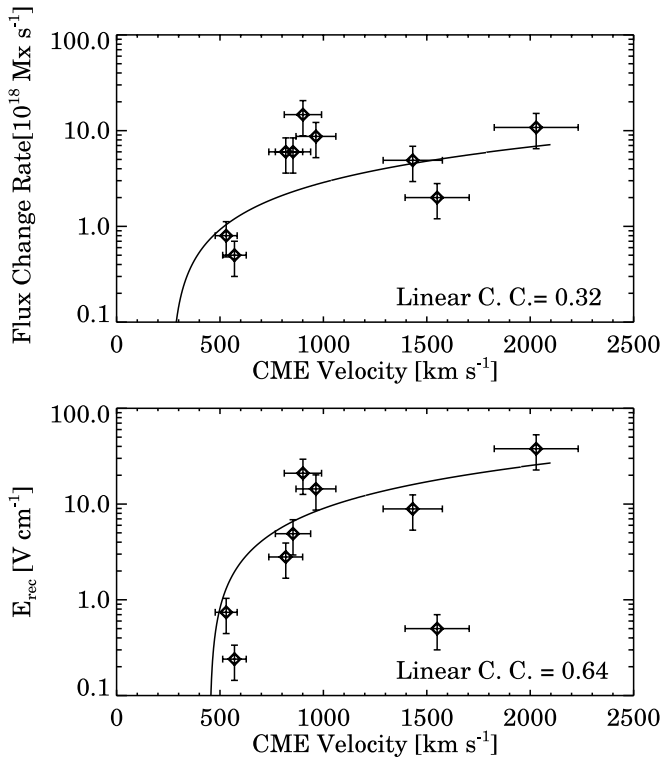


FIG. 5.—*Top*: Scatter diagram of maximum φ_{rec} vs. CME velocity at C2 in a logarithmic scale. The solid line is a fit to the data points of φ_{rec} and V_{CME} in the form of $\varphi_{\text{rec}} = -1.0 + 0.004V_{\text{CME}}$ with a correlation coefficient of 0.32. *Bottom*: Scatter diagram of maximum E_{rec} vs. CME velocity at C2 in a logarithmic scale. The solid line is a fit to the data points of E_{rec} and V_{CME} in the form of $E_{\text{rec}} = -7.3 + 0.02V_{\text{CME}}$ with a correlation coefficient of 0.64. Error bars attached to each point indicate the uncertainty of the measurement.

($V_{\text{CME}} = \int A_{\text{CME}} dt$) and, therefore, in some way conveys information about the acceleration during that stage. Thus, the velocity of CMEs is an alternate way to examine the correlation between the magnetic reconnection rate and the evolution of CMEs. A graphical display of the CME velocity versus the reconnection rate is presented in Figure 5. Inspection of this display immediately reveals that the correlation improved markedly: the paired data V_{CME} and E_{rec} have a moderate CC, 0.64, while the CC for V_{CME} and φ_{rec} , 0.32, implies a low degree of correlation.

5. SUMMARY AND DISCUSSION

Measurements of E_{rec} and φ_{rec} , which both indicate the magnetic reconnection rate inside the current sheet, together with the observational flux-rope acceleration, provide an interesting approach to study the magnetic reconnection rate during the eruptive process. 13 well-observed two-ribbon flares, with corresponding eruptive flux ropes, were studied to investigate and quantify the correlation between the magnetic reconnection rate and flux-rope acceleration. The main results obtained from the sample are summarized as follows:

1. The deduced electric field E_{rec} and the flux change rate φ_{rec} mostly occur in the range of $0.2\text{--}3 \text{ V cm}^{-1}$ and $0.5\text{--}2 \times 10^{18} \text{ Mx}$

s^{-1} , respectively. The magnitude of the *GOES* X-ray flare (expressed in units of W m^{-2}) increases with E_{rec} as shown in Figure 1. The electric field strength found above is enough to accelerate electrons to very high energies, which may account for the strong hard X-ray emissions (Cheng et al. 2003).

2. The magnetic reconnection rate is temporally correlated with the evolution of flare hard X-ray emission and the acceleration of the accompanying erupting filaments. Our results confirm the earlier finding of a good temporal correlation, which is indicative a physical link, between mass acceleration and the magnetic reconnection rate in flares/CMEs (Qiu et al., 2004).

3. The CC between E_{rec} and A_{fila} is about 0.97, and that between φ_{rec} and A_{fila} is about 0.94. Such high values indicate a very strong correlation and a dependable relationship between the magnetic reconnection rate and the acceleration of erupting filaments. The paired data are best fitted to the following linear models: $E_{\text{rec}} = -0.46 + 6.8A_{\text{fila}}$, and $\varphi_{\text{rec}} = 0.26 + 4.6A_{\text{fila}}$.

4. It appears, from our results, that there is no correlation between the magnetic reconnection rate and the CME acceleration (CC is less than 0.2). This may be caused by the temporal-spatial gap between the disk observations of the flares and filaments and LASCO (C2 and C3) observations of CME fronts. From this result, we may infer that CMEs slow down, or even cease, accelerating before they appear in LASCO C2 coronagraph images. Hence, in general, it is less meaningful to compare the magnetic reconnection rate and the CME acceleration.

5. The velocity of CMEs might be an alternate way to investigate the relationship between CMEs and flares that involve magnetic reconnection. When we plot the velocity of CMEs versus the magnetic reconnection rate, the correlation improves somewhat (CC $\sim 0.32\text{--}0.64$), but not enough to make us confident in the relationship between the velocity of CMEs and the magnetic reconnection rate. The reason is that the CME velocity in C2 somewhat conveys the information about the acceleration. The exact acceleration progress below C2 still remains unknown. Another complementary way of looking at this is, in a flare–CME loop–giant arch system, that the separatrix bubble that surrounds the flux rope is the product of magnetic reconnection. During the eruptive progress, the bubble swells much faster than the flux ropes. Therefore, the “flux rope” observed by coronagraphs might actually be the rapidly expanding separatrix bubble (Lin 2004).

We thank Guo Yang, Vasyl Yurchyshyn, and Thomas Spirock for providing the $\text{H}\alpha$ data. We thank Thomas Spirock for his help in improving the contents of this paper. The CME catalog is generated and maintained by NASA and the Catholic University of America in cooperation with the Naval Research Laboratory. *SOHO* is a project of international collaboration between ESA and NASA. J. Jing and H. Wang are supported by NSF under grants ATM-0313591 and ATM-0233931 and by NASA under grants NAG5-12733 and NAG5-13661. J. Qiu is supported by NASA grant NAG0-4GF07G.

REFERENCES

- Amari, T., Luciani, J. F., Aly, J. J., & Tagger, M. 1996, *ApJ*, 466, L39
 Antiochos, S. K., DeVore, C. R., & Klimchuk, J. A. 1999, *ApJ*, 510, 485
 Brueckner, G. E., et al. 1995, *Sol. Phys.*, 162, 357
 Cheng, C. Z., Ren, Y., Choe, G. S., & Moon, Y. J. 2003, *ApJ*, 596, 1341
 Choe, G. S., & Cheng, C. Z. 2000, *ApJ*, 541, 449
 Choudhary, D. P., & Gary, G. A. 1999, *Sol. Phys.*, 188, 345
 Forbes, T. G., & Isenberg, P. A. 1991, *ApJ*, 373, 294
 Forbes, T. G., & Lin, J. 2000, *J. Atmos. Sol.-Terr. Phys.*, 62, 1499
 Forbes, T. G., & Priest, E. R. 1984, in *Solar Terrestrial Physics: Present and Future*, ed. D. M. Butler & K. Papadopoulos (Washington: NASA), 1

- Forbes, T. G., & Priest, E. R. 1995, *ApJ*, 446, 377
- Gonzalez, R. C., & Woods, R. E. 2002, *Digital Image Processing* (Upper Saddle River: Prentice Hall)
- Gopalswamy, N., & Thompson, B. J. 2000, *J. Atmos. Sol.-Terr. Phys.*, 62, 1457
- Gosling, J. T., Hildner, E., MacQueen, R. M., Munro, R. H., Poland, A. I., & Ross, C. L. 1976, *Sol. Phys.*, 48, 389
- Jahne, B. 1997, *Digital Image Processing* (Berlin: Springer)
- Kaastra, J. S. 1985, Ph.D. thesis, Univ. Utrecht
- Lin, J. 2001, Ph.D. thesis, Univ. New Hampshire
- . 2002, *Chinese J. Astron. Astrophys.*, 2, 539
- . 2003, *NewA Rev.*, 47, 53
- . 2004, *Sol. Phys.*, 222, 115
- Lin, J., & Forbes, T. G. 2000, *J. Geophys. Res.*, 105, 2375
- Lin, J., Forbes, T. G., & Isenberg, P. A. 2001, *J. Geophys. Res.*, 106, 25053
- Linker, J., & Mikić, Z. 1994, in *ASP. Conf. Ser. 68, Solar Active Region Evolution: Comparing Models with Observations*, ed. K. S. Balasubramaniam & G. W. Simon (San Francisco: ASP), 251
- MacQueen, R. M., & Fisher, R. R. 1983, *Sol. Phys.*, 89, 89
- Martens, P. C. H., & Kuin, N. P. M. 1989, *Sol. Phys.*, 122, 263
- Martin, S. F. 1989, *Sol. Phys.*, 121, 215
- Mikić, Z., Barnes, D. C., & Schnack, D. D. 1988, *ApJ*, 328, 830
- Neupert, W. M. 1968, *ApJ*, 153, L59
- Poletto, G., & Kopp, R. A. 1986, in *The Lower Atmosphere of Solar Flares*, ed. D. F. Neidig (Sunspot: NSO), 453
- . 1986, *J. Geophys. Res.*, 91, 5579
- Qiu, J., Lee, J., Gary, D. E., & Wang, H. 2002, *ApJ*, 565, 1335
- Qiu, J., Wang, H., Cheng, C. Z., & Gary, D. E. 2004, *ApJ*, 604, 900
- Qu, M., Shih, F., Jing, J., & Wang, H. 2003, *Sol. Phys.*, 217, 157
- . 2004, *Sol. Phys.*, 222, 137
- Shanmugaraju, A., Moon, Y. J., Dryer, M., & Umapathy, S. 2003, *Sol. Phys.*, 215, 185
- Van Tend, W., & Kuperus, M. 1978, *Sol. Phys.*, 59, 115
- Wang, H. 2005, *ApJ*, 618, 1012
- Wang, H., Qiu, J., Jing, J., Spirock, T. J., & Yurchyshyn, V. 2004, *ApJ*, 605, 931
- Wang, H., Qiu, J., Jing, J., & Zhang, H. 2003, *ApJ*, 593, 564
- Xu, Y., Cao, W., Liu, C., Yang, G., Qiu, J., Jing, J., Denker, C., & Wang, H. 2004, *ApJ*, 607, L131
- Zhang, J., Dere, K. P., Howard, R. A., Kundu, M. R., & White, S. M. 2001, *ApJ*, 559, 452